Empirical tight-binding calculation of dispersion in the second-order nonlinear optical constant for zinc-blende crystals

D. J. Moss, J. E. Sipe, and H. M. van Driel
Department of Physics, University of Toronto, Toronto, Canada M5S 1A7
(Received 15 June 1987)

We calculate both the finite- and zero-frequency values of $\vec{\chi}^{(2)}$ for the zinc-blende materials GaP, GaAs, GaSb, InAs, and InSb, by employing an empirical tight-binding band-structure technique, used previously to obtain the dispersion in the linear-optical properties. The momentum matrix elements are calculated by three methods: by using $\mathbf{k}\cdot\mathbf{p}$ perturbation theory together with the experimental effective masses, by direct calculation using wave functions from a more fundamental theory, and by fitting $\epsilon_1(0)$ to experiment. The calculated conduction-band–conduction-band (c-c) momentum matrix elements were found to be approximately an order of magnitude smaller than the experimental matrix elements, while the valence-band–conduction-band (v-c) matrix elements agreed much better. When the experimental c-c matrix elements are used, good agreement is found between theory and experiment for $\vec{\chi}^{(2)}$ for all materials except InAs and InSb in the low-frequency region. For these latter materials, the discrepancy is accounted for by inadequacies in the empirical tight-binding band structure. It is proposed that Fong and Shen's [Phys. Rev. B **12**, 2325 (1975)] anomalously low results for $\vec{\chi}^{(2)}(0)$ could be due to calculated values for the c-c (or v-c) momentum matrix elements which are too small.

I. INTRODUCTION

Calculation of the dispersion in the nonlinear-optical properties of solids requires detailed information about the band structure and wave functions throughout the Brillouin zone (BZ). The first attempt to calculate the dispersion in $\vec{\chi}^{(2)}$ for second-harmonic generation (SHG) in zinc-blende crystals was by Bell[1] in 1972. He avoided the use of a full band-structure calculation by phenomenologically modeling the bands only around a few principal critical points, the points responsible for the main features in the linear-optical absorption spectrum. Since then, Fong and Shen[2] (FS) have employed a pseudopotential band-structure calculation of $\vec{\chi}^{(2)}$ in three zinc-blende materials—GaAs, InAs, and InSb—and compared their results with Bell's. They found that, in general, the agreement with experiment was improved over Bell's results, and the main experimental features in the spectrum of $\vec{\chi}^{(2)}$ were present in the theoretical curves. However, significant differences still existed between theory and experiment. In particular, for all three compounds their results for the zero-frequency values of $\vec{\chi}^{(2)}$ were over an order of magnitude smaller than the corresponding experimental values. In addition, there were differences in the relative size of several peaks in $\vec{\chi}^{(2)}$, and slight discrepancies in the position of the peaks. FS attributed their underestimate of the zero-frequency limit of $\vec{\chi}^{(2)}$ to their neglect of local field effects, dismissing the possibility that the calculated momentum matrix elements were too small.

In this paper we employ an empirical tight-binding (ETB) band-structure calculation of $\vec{\chi}^{(2)}(\omega)$ for the zinc-blende materials GaP, GaAs, GaSb, InAs, and InSb, focusing in particular on the compounds GaAs, InAs, and InSb, for which dispersion measurements have been made.[3–6] Although for semiconductors plane-wave based band structure methods [such as the empirical pseudopotential method (EPM)], in general yield more accurate results than that for ETB techniques, the ETB approach has the advantage of being substantially simpler, and applicable to a wide variety of materials, including even amorphous semiconductors. Previously[7] we used an ETB band-structure method to calculate the dispersion in the linear-optical absorption spectrum for a variety of semiconductors, with good results for most materials, and it is of interest to determine how well ETB techniques can be used to calculate the nonlinear-optical properties of solids.

This paper has two other main objectives. First, an alternative to the method of FS's for calculating $\vec{\chi}^{(2)}$ is adopted. Theoretical expressions for the real and imaginary parts of $\vec{\chi}^{(2)}$ are presented which do not display singular behavior in the limit of $\omega\rightarrow 0$. The imaginary part of $\vec{\chi}^{(2)}$ is evaluated first, using an extension of the linear analytic tetrahedra method (LATM) for zone integration,[8] to nonlinear response functions.[9] The real part of $\vec{\chi}^{(2)}$ is obtained by using the Kramers-Kronig relations on the imaginary part, as in evaluating the linear response function. Beginning with an evaluation of the imaginary part of $\vec{\chi}^{(2)}$ has two main advantages. It simplifies the calculation in the same manner as when evaluating the linear dielectric function, and it exhibits $\vec{\chi}^{(2)}$ in a form which can be related simply to the linear imaginary dielectric constant $[\epsilon_2(\omega)]$ at ω and 2ω, thus permitting easier correlations between critical points in the band structure and structures in $\vec{\chi}^{(2)}(\omega)$. Finally, attention is focused on the zero-frequency limit of $\vec{\chi}^{(2)}$ in an effort to understand why FS's results consistently underestimated $\vec{\chi}^{(2)}$ $(\omega\rightarrow 0)$ while all other theories,[1,10–13]

albeit not full band-structure techniques, do not. This point is important, since nonlinear local-field effects in solids are not understood, and FS claim that local-field effects are important for nonlinear response functions in solids, whereas they are known[14] to have a relatively minor effect on the linear-optical spectrum of covalent solids. Since the magnitude of $\vec{\chi}^{(2)}$ depends on momentum matrix elements to the third power, it is clear that if one wishes to establish if local-field effects are indeed important, one must first be confident that the magnitude of the matrix elements is correct. To this end we calculate the momentum matrix elements using three different approaches. We obtain the experimental momentum matrix elements from the observed effective masses at the Brillouin zone center, as other authors have done.[1,13,15] The second method is to calculate the matrix elements using tight-binding wave functions from a more fundamental theory.[16] Finally, the valence-band–conduction-band (v-c) matrix elements are determined by fitting the calculated value of the dielectric constant at zero frequency [$\epsilon_1(0)$] to experiment. In the case of conduction-band–conduction-band (c-c) matrix elements, an independent means of determining them, such as fitting $\epsilon_1(0)$, is not available. Only the experimental values and the values calculated from the wave functions are available.

Our results show that the values for the (v-c) matrix elements obtained by fitting $\epsilon_1(0)$ to experiment are consistently $\sim$20–30 % smaller than the experimental matrix elements, but agree reasonably well with the values calculated from the wave functions. The values for the c-c matrix elements calculated from the wave functions, on the other hand, were smaller than the experimentally determined values by, in some cases, over an order of magnitude. Clearly then, the approach of using the calculated matrix elements and the approach of using the experimental matrix elements would in our case yield results for $\vec{\chi}^{(2)}(0)$ which differ by over an order of magnitude. We feel that this, rather than the neglect of local-field corrections, could be the reason for FS's anomalously low calculated values for $\vec{\chi}^{(2)}(0)$. In our calculation for $\vec{\chi}^{(2)}$, we used the values for the (v-c) matrix elements determined from the last method (which agreed fairly well with the second method for most compounds), and values for the c-c matrix elements determined from the first method (since the second method yielded poor results, and the last method was inapplicable). Our results show that for compounds where the linear-optical properties are well predicted, the values for $\vec{\chi}^{(2)}(0)$ agree well with experiment.

Agreement between theory and experiment for the dispersion in $\vec{\chi}^{(2)}$ is good for GaAs, and fair for InAs and InSb. The ETB band-structure calculations had the most difficulty in reproducing pseudopotential bands for InAs and InSb, and consequently our results for $\vec{\chi}^{(2)}(\omega)$ are not surprising. There exist differences between theory and experiment even for pseudopotential[2] calculations and for our calculations (for all compounds); however, in view of the degree to which the experimental data in the literature varies, a conclusive evaluation of the theory is difficult.

Therefore, we see that for cases where the linear-optical properties are well reproduced, empirical tight-binding methods can indeed be used to calculate the dispersion of nonlinear parameters. In cases where the calculated linear properties are not as good, the discrepancies in the dispersion of the nonlinear-optical properties are naturally larger. This demonstrates that the dispersion in nonlinear parameters can be used as more sensitive tests of band-structure theories, notwithstanding the difficulty in making measurements of nonlinear properties.

The rest of the paper is organized as follows. In Sec. II the theoretical expressions for the real and imaginary parts of $\vec{\chi}^{(2)}$ are presented in a form which is nondivergent in the zero-frequency limit. In Sec. III the method of calculation of $\vec{\chi}^{(2)}$ is discussed (without reference to the momentum matrix elements), and in Sec. IV the three methods for determining the momentum matrix elements are presented. In Sec. V the results for the matrix elements $\vec{\chi}^{(2)}(0)$ and dispersion in $\vec{\chi}^{(2)}$ are presented and discussed. Finally, in Sec. VI a brief summary is given.

II. THEORY

The theoretical expression for $\vec{\chi}^{(2)}$ is obtained from standard perturbation theory[17] and, for second-harmonic generation, the expression reduces in the case of cubic symmetry to

$$\vec{\chi}^{(2)}(\omega)=\frac{i}{2}\left|\frac{e}{m\omega}\right|^3 \sum_{i,j,l}{}' \int_{\mathrm{BZ}} \frac{d\mathbf{k}}{4\pi^3}\{\mathbf{p}_{ij}\mathbf{p}_{jl}\mathbf{p}_{li}\}\left\{\frac{1}{(E_{ji}-2E)(E_{li}-E)}+\frac{1}{(E_{li}+2E)(E_{ji}+E)}+\frac{1}{(E_{ji}+E)(E_{li}-E)}\right\}, \tag{1}$$

[where $E_{ji}=E_j-E_i$, etc., $E=\hbar\omega+i\eta$ ($\eta\to 0$), and the $\sum'_{ijl}$ means that i must label an occupied valence-band state and $j\neq l$ are conduction band indices. This contribution, therefore, is a three-band term. There is a one-band contribution ($i=j=l$ and all three refer to a valence band) which vanishes identically, and a two-band contribution ($i=j\neq l$; $i=l\neq j$ where, e.g., if $i=j$, then i refers to a valence-band state and l refers to a conduction-band state) which vanishes when inversion symmetry of the Brillouin zone (time-reversal symmetry) is used. All of these contributions have been discussed in detail by Aspnes.[13] In addition, there is the contribution of the virtual hole process to consider. For the virtual electron process the three-band expression requires that i = valence band, j,l = conduction-band states, so we have a valence-band–conduction-band–conduction-band (or v-c-c') transition. For the virtual hole process, we have a v-v'-c transition. Aspnes[13] considered this term and demonstrated that, for the materials dealt with

in this paper, it will be negative and more than an order of magnitude smaller than that of the virtual electron process. We therefore ignore the virtual hole contribution in this paper.

When inversion symmetry is explicitly included for the three-band term, one has[1,13] $\mathbf{p}_{ij}(\mathbf{k})=-\mathbf{p}_{ij}^{*}(-\mathbf{k})=-\mathbf{p}_{ji}(-\mathbf{k})$ so that putting $\mathbf{k}\rightarrow-\mathbf{k}$ is equivalent to interchanging j and l and multiplying by -1. The expression for $\vec{\vec{\chi}}^{(2)}$ becomes

$$\vec{\vec{\chi}}^{(2)}(\omega)=\frac{i}{2}\left|\frac{e\hbar}{m}\right|^{3}\sum_{i,j,l}{}'\int_{\mathrm{BZ}}\frac{d\mathbf{k}}{4\pi^{3}}\{\mathbf{p}_{ij}\mathbf{p}_{jl}\mathbf{p}_{li}\}\frac{1}{E^{2}}\left\{\frac{(E_{ji}+2E_{li})}{(E_{ji}^{2}-4E^{2})(E_{li}^{2}-E^{2})}-\frac{(2E_{ji}+E_{li})}{(E_{li}^{2}-4E^{2})(E_{ji}^{2}-E^{2})}+\frac{(E_{ji}-E_{li})}{(E_{ji}^{2}-E^{2})(E_{li}^{2}-E^{2})}\right\}. \tag{2}$$

If this expression is separated into partial fractions, the terms $1/E$ and $\sim 1/E^{2}$ vanish identically (without employing sum rules) and so the remaining expression is explicitly nondivergent as $E\rightarrow 0$. To obtain the real and imaginary parts of Eq. (2), one puts $E=\hbar\omega+i\eta$ and takes the limit as $\eta\rightarrow 0$, in the same manner as for the linear response function. From time-reversal symmetry we have

$$\{\mathbf{p}_{ij}\mathbf{p}_{jl}\mathbf{p}_{li}\}_{\mathbf{k}}+\left\{\ \right\}_{-\mathbf{k}}=\left\{\ \right\}_{\mathbf{k}}-\left\{\ \right\}_{\mathbf{k}}^{*}\sim i\ \mathrm{Im}\left\{\ \right\}_{\mathbf{k}}, \tag{3}$$

so that only the imaginary part of the matrix element product survives. Therefore, $\vec{\vec{\chi}}^{(2)}$ can be written as

$$\vec{\vec{\chi}}^{(2)}(\omega)=\vec{\vec{\chi}}^{(2)'}(\omega)+i\vec{\vec{\chi}}^{(2)''}(\omega), \tag{4}$$

where $\vec{\vec{\chi}}^{(2)'}$ and $\vec{\vec{\chi}}^{(2)''}$ are both real, and given by

$$\vec{\vec{\chi}}^{(2)'}(\omega)=+\frac{i}{2}\left|\frac{\hbar e}{m}\right|^{3}\sum_{i,j,l}{}'\int\frac{d\mathbf{k}}{4\pi^{3}}\{\mathbf{p}_{ij}\mathbf{p}_{jl}\mathbf{p}_{li}\}\left\{\frac{16}{E_{ji}^{2}(2E_{li}-E_{ji})(E_{ji}^{2}-4E^{2})}+\frac{(2E_{li}-E_{ji})}{E_{ji}^{2}(2E_{ji}-E_{li})(E_{ji}^{2}-E^{2})(E_{ji}+E_{li})}-(j\leftrightarrow l)\right\}, \tag{5a}$$

$$\vec{\vec{\chi}}^{(2)''}(\omega)=+\frac{\pi}{4}i\left|\frac{\hbar e}{m}\right|^{3}\sum_{i,j,l}{}'\int\frac{d\mathbf{k}}{4\pi^{3}}\{\mathbf{p}_{ij}\mathbf{p}_{jl}\mathbf{p}_{li}\}\left\{\frac{16\delta(E_{ji}-2E)}{E_{ji}^{3}(2E_{li}-E_{ji})}+\frac{(2E_{li}-E_{ji})\delta(E_{ji}-E)}{E_{ji}^{3}(2E_{ji}-E_{li})(E_{ji}+E_{li})}-(j\leftrightarrow l)\right\}, \tag{5b}$$

in agreement with earlier results.[18] It is straightforward to verify that $\vec{\vec{\chi}}^{(2)'}(\omega)$ and $\vec{\vec{\chi}}^{(2)''}(\omega)$ satisfy the Kramers-Kronig relations, as required by causality,[19,20] viz.

$$\vec{\vec{\chi}}^{(2)'}(\omega)=\frac{2}{\pi}\mathrm{P}\int_{0}^{\infty}\frac{\omega'}{\omega'^{2}-\omega^{2}}\vec{\vec{\chi}}^{(2)''}(\omega')d\omega', \tag{6}$$

and the corresponding inverse relation, where P refers to the principal part of the integral. Thus one need only evaluate $\vec{\vec{\chi}}^{(2)''}$ from a band-structure calculation. As in the case of the linear susceptibility, the imaginary part of $\vec{\vec{\chi}}^{(2)}$ is substantially simpler to evaluate than the real part, owing to the presence of the Dirac δ functions.

We next consider the structure in $\vec{\vec{\chi}}^{(2)''}$ to be expected from a given band structure. One can see from Eq. (5b) that $\vec{\vec{\chi}}^{(2)''}$ contains two pieces, one which is similar in nature to $\epsilon_2(2\omega)$ and one which is similar to $\epsilon_2(\omega)$. We call the first term, which is $\sim\delta(E_{ji}-2E)$, the 2ω term and the second term, which is $\sim\delta(E_{ji}-E)$, the ω term. If the coefficients in front of the δ functions were constant, then (ignoring any $\mathbf{k}$ dependence of the momentum matrix elements) $\vec{\vec{\chi}}^{(2)''}$ would simply be the sum of terms proportional to $\epsilon_2(\omega)$ and $\epsilon_2(2\omega)$, and in fact this was the basis for simplified models[2,3] used to determine the spectrum of $\vec{\vec{\chi}}^{(2)}(\omega)$. It is evident from Eq. (5b) that $\vec{\vec{\chi}}^{(2)''}$ will also show "double resonance" structure when $E_{ji}\sim 2E_{li}$ for the 2ω term, or when $E_{li}\sim 2E_{ji}$ for the ω term. Consider first the 2ω term. If E_{ji} has a critical point at 2ω, but E_{li} does not (at the same point in the BZ), then if the double resonance condition is satisfied only rapid oscillations of $\vec{\vec{\chi}}^{(2)''}$ will result. This is observed in practice for almost all materials; however, this does not result in a large peak. If, on the other hand, E_{li} also has a critical point (at the same point in the BZ), and the double resonance condition is satisfied, then the response can be greatly enhanced, being either positive or negative depending on whether $2E_{li}$ is less than or greater than E_{ji} at the critical point. This last condition is much more unlikely, and we presume that this is the condition implied by FS in their discussion of InSb. We reserve the term double resonance to apply to this last case. The same argument holds true for the ω term, with E_{ji} resonant at $\hbar\omega$ and with $E_{li}\sim 2E_{ji}$. Hence, contrary to what one may expect, the double resonance structure occurs where *both* $\epsilon_2(2\omega)$ and $\epsilon_2(\omega)$ have structure, not where neither of them have structure.

Another quantity of interest, both experimentally and theoretically, is $\vec{\vec{\chi}}^{(2)}(0)$. Letting $\omega\rightarrow 0$ in Eq. (5a) and rearranging this expression we obtain

$$\overleftrightarrow{\chi}^{(2)'}(0)=+\tfrac{3}{2}i\left|\frac{e\hbar}{m}\right|^3\sum_{i,j,l}{}'\int_{\mathrm{BZ}}\frac{d\mathbf{k}}{4\pi^3}\{\mathbf{p}_{ij}\mathbf{p}_{jl}\mathbf{p}_{li}\}\left[\frac{E_{li}^2(2E_{li}+E_{ji})-E_{ji}^2(2E_{ji}+E_{li})}{E_{ji}^4E_{li}^4}\right], \tag{7}$$

which agrees with Aspnes'[21] result (note that Aspnes[13,21] uses $e=+|e|$ whereas other authors[1,2] have used $e=-|e|$). This expression is simpler to evaluate than $\overleftrightarrow{\chi}^{(2)}(\omega)$ primarily because it involves no resonance denominators, and hence can be used as a check for the results of $\overleftrightarrow{\chi}^{(2)'}(\omega)$ and $\overleftrightarrow{\chi}^{(2)''}(\omega)$. From Sec. IV it will be seen that at the Γ point ($\mathbf{k}=\mathbf{0}$), $\{\mathbf{p}_{ij}\mathbf{p}_{jl}\mathbf{p}_{li}\}\sim -iA(\hbar/a_b)^3$ where A is a positive real (dimensionless) constant, i refers to the top three (degenerate) valence bands, j refers to the bottom (s-like) conduction band, and l refers to the top three (degenerate) conduction bands which are p like. Therefore, as Aspnes[13] pointed out, if $E_{li}>E_{ji}$, as it is in all of the materials we studied, one will obtain $\overleftrightarrow{\chi}^{(2)}(0)>0$, as observed.

III. METHOD OF CALCULATION

We evaluate $\overleftrightarrow{\chi}^{(2)}$ employing ETB bands used previously[7] to calculate the dispersion in the linear-optical properties with good success. We refer the reader to that paper for the formalism of the model and the results of the calculation. The ETB method does not provide detailed information about wave functions, and we defer the discussion of the determination of the momentum matrix elements until the next section.

In order to integrate Eq. (5b) over the irreducible BZ segment, we employ an extension of the linearized analytic tetrahedral method (LATM) (Ref. 9) to the nonlinear response function. The details of the application of this method are presented elsewhere, and only a brief summary and the results of the method will be presented here. The bands are linearized over tetrahedral cells with the energy derivatives determined by the band energies at the tetrahedra vertices. The integration of Eq. (5b) over a tetrahedral cell can then be carried out analytically, and it is found that the result (as in the linear case) is independent of the geometry of the cell. The result is

$$\overleftrightarrow{\chi}^{(2)''}(\omega)=\overleftrightarrow{C}\sum_{\substack{\gamma\\ \text{Irreducible zone}}}g_\gamma(\omega), \tag{8}$$

where $C_{ijk}=0$ unless $i\neq j\neq k$ and unity otherwise, and $g_\gamma(\omega)$ is the contribution of one tetrahedron in the irreducible zone to $\overleftrightarrow{\chi}^{(2)}(\omega)$, taking into account the 48-fold symmetry of the zone. We explicitly write the result for $g_\gamma(\omega)$ in esu units which, using the results from the last section, is

$$g_\gamma(\omega)=-\frac{4.32\times10^{-5}}{8\pi^2}\left[\frac{2\ \mathrm{Ry}}{\hbar\omega}\right]^3\frac{6v'}{a_0'^3}\sum_{i,j,l}F_{ijl}(\mathbf{k})[g_1(\mathbf{k})\delta(E_{ji}-2\hbar\omega)+g_2(\mathbf{k})\delta(E_{ji}-\hbar\omega)], \tag{9}$$

where 2 Ry=27.212 eV, all energies on the right are in eV, $a_0'=a_0/a_b$ with a_0 being the lattice constant, a_b is the Bohr radius, and v' is the dimensionless volume ($a_0=1$) of the tetrahedron. [The factor of 4.32×10^{-5} arises because $\overleftrightarrow{\chi}^{(2)}$ has dimensions of (e^3/E^2) where E is energy, and $(e^3/E^2)_{\mathrm{esu}}=4.32\times10^{-5}/(E)^2_{\mathrm{eV}}$.] Here $F_{ijl}(\mathbf{k})$ is defined by

$$\sum_R P_R(\{\mathbf{p}_{ij}\mathbf{p}_{jl}\mathbf{p}_{li}\})\equiv\overleftrightarrow{C}F_{ijl}(\mathbf{k})i\left[\frac{\hbar}{a_b}\right]^3, \tag{10}$$

where $\sum_R P_R$ indicates a sum over the 48 transformation operators of the cubic group. Note that the inversion operator is included since the Brillouin zone has inversion symmetry, even though the direct lattice does not. With this definition $F_{ijl}(\mathbf{k})$ is real and dimensionless.

The 48-fold symmetry of the BZ is taken into account by the following. The set of cubic transformation operators ($\sum_R P_R$) operating on the matrix element product appearing in Eq. (5) give

$$\sum_R P_R\{\mathbf{p}_{ij}\mathbf{p}_{jl}\mathbf{p}_{li}\}=8\overleftrightarrow{C}\{p_{ij}^xp_{jl}^yp_{li}^z+p_{ij}^xp_{jl}^zp_{li}^y+p_{ij}^yp_{jl}^xp_{li}^z+p_{ij}^yp_{jl}^zp_{li}^x+p_{ij}^zp_{jl}^xp_{li}^y+p_{ij}^zp_{jl}^yp_{li}^x\}, \tag{11}$$

where $\overleftrightarrow{C}$ is the tensor appearing in Eq. (8), and only the imaginary part of the product is evaluated. Therefore, there is only one independent element for $\overleftrightarrow{\chi}^{(2)}$ in cubic materials, namely $\chi^{(2)}_{123}$.

In Eq. (9), $g_1(\mathbf{k})$ and $g_2(\mathbf{k})$ are determined by which region of the tetrahedron E_{ji} falls in. The regions are defined by

$$\varepsilon_0^{(m)}\leq\varepsilon^{(m)}\leq\varepsilon_1^{(m)}\quad(\text{region I}),$$

$$\varepsilon_1^{(m)}\leq\varepsilon^{(m)}\leq\varepsilon_2^{(m)}\quad(\text{region II}),$$

$$\varepsilon_2^{(m)}\leq\varepsilon^{(m)}\leq\varepsilon_3^{(m)}\quad(\text{region III}),$$

where $\varepsilon^{(m)}\equiv E_{ji}$ and $\varepsilon_0^{(m)}$, $\varepsilon_1^{(m)}$, $\varepsilon_2^{(m)}$, and $\varepsilon_3^{(m)}$ are the energies (E_{ji}) at the vertices of the tetrahedron in ascending or-

der. We will simply list the result if E_{ji} is in region I, and refer the reader elsewhere[9] for the results from the other regions. For region I, we have

$$g_1(\mathbf{k})=\left[\frac{\varepsilon^{(m)}-2\varepsilon_{s'}^{(n)}}{2}\right]\left|\frac{\varepsilon_{s0}^{(m)}}{\Delta_{su}\Delta_{st}}\right|\ln\left|\frac{2\varepsilon_{t'}^{(n)}-\varepsilon^{(m)}}{2\varepsilon_{s'}^{(n)}-\varepsilon^{(m)}}\right|+\left[\frac{\varepsilon^{(m)}-2\varepsilon_{u'}^{(n)}}{2}\right]\left|\frac{\varepsilon_{u0}^{(m)}}{\Delta_{su}\Delta_{tu}}\right|\ln\left|\frac{2\varepsilon_{t'}^{(n)}-\varepsilon^{(m)}}{2\varepsilon_{u'}^{(n)}-\varepsilon^{(m)}}\right|, \tag{12a}$$

and

$$g_2(\mathbf{k})=\left|\frac{\varepsilon_{s0}^{(m)}}{\Delta_{su}\Delta_{st}}\right|\left[(\varepsilon_{s'}^{(n)}+\varepsilon^{(m)})\ln\left|\frac{\varepsilon_{t'}^{(n)}+\varepsilon^{(m)}}{\varepsilon_{s'}^{(n)}+\varepsilon^{(m)}}\right|+(2\varepsilon^{(m)}-\varepsilon_{s'}^{(n)})\ln\left|\frac{2\varepsilon^{(m)}-\varepsilon_{s'}^{(n)}}{2\varepsilon^{(m)}-\varepsilon_{t'}^{(n)}}\right|\right]$$
$$+\left|\frac{\varepsilon_{u0}^{(m)}}{\Delta_{us}\Delta_{ut}}\right|\left[(\varepsilon_{u'}^{(n)}+\varepsilon^{(m)})\ln\left|\frac{\varepsilon_{t'}^{(n)}+\varepsilon^{(m)}}{\varepsilon_{u'}^{(n)}+\varepsilon^{(m)}}\right|+(2\varepsilon^{(m)}-\varepsilon_{u'}^{(n)})\ln\left|\frac{2\varepsilon^{(m)}-\varepsilon_{u'}^{(n)}}{2\varepsilon^{(m)}-\varepsilon_{t'}^{(n)}}\right|\right], \tag{12b}$$

where $\varepsilon^{(n)}=E_{li}$, and $\varepsilon_{s'}^{(n)}$, $\varepsilon_{t'}^{(n)}$, and $\varepsilon_{u'}^{(n)}$ are the energies in ascending order at the corners of the triangle consisting of the plane $E_{ji}=\varepsilon^{(m)}=\text{const}$ inside the tetrahedra. The remaining quantities in Eq. (12) are defined as

$$\begin{aligned}\Delta_{us}&=\varepsilon_{u0}^{(m)}\varepsilon_{s0}^{(n)}-\varepsilon_{s0}^{(m)}\varepsilon_{u0}^{(n)},\\ \Delta_{ut}&=\varepsilon_{u0}^{(m)}\varepsilon_{t0}^{(n)}-\varepsilon_{t0}^{(m)}\varepsilon_{u0}^{(n)},\\ \Delta_{st}&=\varepsilon_{s0}^{(m)}\varepsilon_{t0}^{(n)}-\varepsilon_{t0}^{(m)}\varepsilon_{s0}^{(n)},\end{aligned} \tag{13}$$

and

$$\varepsilon_{u0}^{(m)}=\varepsilon_{u}^{(m)}-\varepsilon_{0}^{(m)},\quad\text{etc.},$$

where $\varepsilon_u^{(m)}$ is the energy E_{ji} evaluated at point u, defined as the $\mathbf{k}$ vector of the tetrahedron vertex on the line $\mathbf{k}_{u'}-\mathbf{k}_0$, and similarly for $\varepsilon_s^{(m)}$, $\varepsilon_t^{(m)}$.

The integration is carried out by dividing the irreducible BZ segment into parallelepipeds and further dividing these into six constituent tetrahedra. The matrix elements are assumed constant over all tetrahedra within the same parallelepiped. This scheme has the obvious advantage that a factor of 6 is gained in resolution without having to diagonalize the Hamiltonian at any points other than the parallelepiped vertices. The disadvantage to this scheme is that the irreducible BZ is not evenly divisible into parallelepipeds. The BZ boundary is accounted for by including the tetrahedron contribution if at least two of its vertices are inside the BZ and excluding it otherwise. Using this scheme, when the band energies are obtained at 88 points in the irreducible BZ, the volume obtained is correct to better than 1%. In addition, the calculations are performed with an energy resolution of 0.05 eV, and so any structure in $|\vec{\chi}^{(2)}|$ on this scale is likely due to numerical artifacts.

IV. MOMENTUM MATRIX ELEMENTS

Since the magnitude of $\vec{\chi}^{(2)}$ depends directly on the values chosen for the momentum matrix elements, we devote considerable attention to the determination of these matrix elements. Three approaches are considered to determine the matrix elements: (1) we use a semiempirical model introduced by Cardona[15] and used by Bell[1] and Aspnes,[13] together with experimental data of the conduction-band effective masses, to determine the matrix elements at the Brillouin zone center [this can be applied to both the (v-c) and (c-c) momentum matrix elements]; (2) we calculate the matrix elements using wave-function orbitals obtained from a more elaborate band-structure calculation;[16] (3) we calculate the (v-c) type matrix elements only to a particular nearest neighbor and then adjust the matrix element, using only one scaling factor, at the Brillouin zone center to yield the experimental value for $[\epsilon_1(0)]$. Clearly this last approach can only be applied to the v-c type matrix elements, since the c-c matrix elements do not appear in the expressions for $\epsilon_1(\omega)$. Below, we briefly outline in detail each of these three approaches.

The approach taken to experimentally determine the matrix elements was first introduced by Cardona.[15] First, an expression is obtained from $\mathbf{k}\cdot\mathbf{p}$ perturbation theory[22] for the effective mass at the Γ point of the lowest conduction band, which is nondegenerate (s like) in all the materials studied. Figure 1 shows the band structure obtained for GaAs along with our notation. For nonpolar materials, the matrix element between the

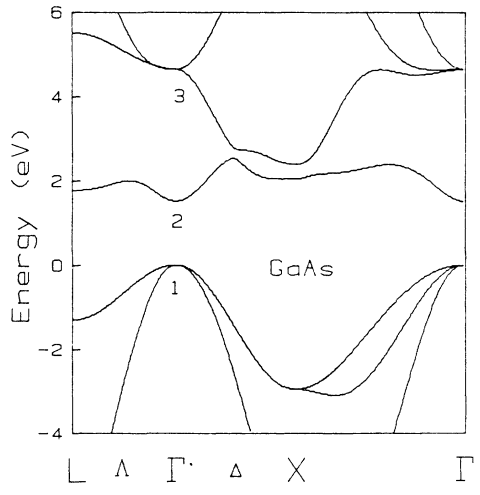

FIG. 1. Band structure for GaAs from Ref. 7. The notation used for the band energies at Γ is as follows. Points 1, 2, and 3 are denoted as $\Gamma_{15}^{v}(\Gamma_{25'}^{v})$, $\Gamma_1^c(\Gamma_{2'}^c)$, and $\Gamma_{15}^c(\Gamma_{15'}^c)$ for polar (nonpolar) solids. In addition, the lowest valence-band point (not shown) is denoted by $\Gamma_1^v(\Gamma_{1'}^v)$.

$\Gamma_{15'}^c$ and $\Gamma_{2'}^c$ bands is zero at the zone center, so the effective mass for the lowest (nondegenerate) conduction band can be written

$$\frac{m}{m_{ij}^*}=\delta_{ij}\left[1+\frac{1}{3}\frac{2}{m}\mid\langle\Gamma_{25'}^v\mid\mathbf{p}\mid\Gamma_{2'}^c\rangle\mid^2\times\left[\frac{2}{E_0}+\frac{1}{E_0+\Delta_0}\right]\right], \tag{14}$$

where cubic symmetry has been assumed, E_0 is the direct energy gap $[=E(\Gamma_{2'}^c)-E(\Gamma_{25'}^v)]$ and Δ_0 (>0) is the energy of the split-off valence band at Γ. This allows one to determine $\mid\langle\Gamma_{25'}^v\mid\mathbf{p}\mid\Gamma_{2'}^c\rangle\mid$ for the nonpolar materials, given the experimental effective masses. For polar materials, Cardona introduced an empirical model wherein the $\Gamma_{15'}^c$, $\Gamma_{25'}^v$ bands in a fictitious nonpolar solid interact via an antisymmetric perturbing potential, V. Only the results from that model, and Aspnes' adaptation of it, will be presented here. We have

$$\langle\Gamma_{15}^v\mid\mathbf{p}\mid\Gamma_1^c\rangle_{\text{polar}}=+iAP\hat{p}\ , \tag{15a}$$

$$\langle\Gamma_{15}^v\mid\mathbf{p}\mid\Gamma_{15}^c\rangle_{\text{polar}}=-iQ\hat{p}\ , \tag{15b}$$

$$\langle\Gamma_1^c\mid\mathbf{p}\mid\Gamma_{15}^c\rangle_{\text{polar}}=+i\frac{VA}{W_c}P\hat{p}\ , \tag{15c}$$

where

$$A=\left[1+\left[\frac{V}{W_c}\right]^2\right]^{-1/2}, \tag{15d}$$

$$W_c=\tfrac{1}{2}[E_1+(E_1^2+4V^2)^{1/2}]\ ,$$

$$V=\tfrac{1}{2}[(E_1^p)^2-E_1^2]^{1/2}\ ,$$

E_1 is the energy of the $\Gamma_{15'}^c$ point in the fictitious nonpolar solid, E_1^p is the energy of the Γ_{15}^c point (relative to the valence-band maximum) in the polar material, and Eq. (15) serves as the definition for P and Q. In Eq. (15), $\hat{p}$ is a unit vector in the appropriate direction, different for each matrix element. For notational convenience, we refer to the matrix elements in Eqs. (15) as v-c, v-c', and c-c', respectively. Note that since $\langle\Gamma_1^v\mid\mathbf{p}\mid\Gamma_1^c\rangle=0$ even for polar materials, the three matrix elements appearing in Eq. (15) are sufficient to determine $\overleftrightarrow{\chi}^{(2)}$ if the matrix elements are assumed to be constant. The result is that at the Γ point $\{\mathbf{p}_{ij}\mathbf{p}_{jl}\mathbf{p}_{li}\}=-iA\{\hat{x}\hat{y}\hat{z}\}(\hbar/a_b)^3$ where A is a positive real dimensionless constant, and $\{\hat{x}\hat{y}\hat{z}\}$ means some permutation of $\hat{x}\hat{y}\hat{z}$, depending on which of the degenerate Γ_{15}^v, Γ_{15}^c bands are present. The matrix elements and band-gap energies (E_1) for the fictitious homopolar solids can be obtained by using the results from Si, Ge etc., and an interpolation scheme which assumes that the matrix elements and band-gap energy E_1 depend only on the lattice constant. Aspnes in fact did this, and we adopt the same interpolation scheme as his. The matrix element $\langle\Gamma_{15}^v\mid\mathbf{p}\mid\Gamma_{15}^c\rangle$ must be obtained from the experimental determination of the valence bands at Γ, which are significantly more complicated than the Γ_1^c conduction band.[15] In addition, the values for this matrix element vary by less than 10% from element to element[1,13] and in fact Cardona assumed the same value of this matrix element for all materials. Therefore, we do not present the details of the determination of this matrix element. Once the matrix elements for nonpolar materials are determined, the matrix elements for the polar materials can be obtained, and the effective mass at the Γ_1^c point calculated and compared with experiment. The equation for the effective mass at Γ_1^c for polar materials is[15]

$$\frac{m}{m^*}(\Gamma_1^c)=1+\frac{1}{m}\frac{\mid\langle\Gamma_{25'}^v\mid\mathbf{p}\mid\Gamma_{2'}^c\rangle\mid^2_{\text{nonpolar}}}{E_1^p}\left[\frac{1}{3}(E_1^p+E_1)\left[\frac{2}{E_0^p}+\frac{1}{E_0^p+\Delta_0^p}\right]-\frac{(E_1^p-E_0)}{\Delta E_c^p}\right], \tag{16}$$

where

$$E_0^p=E(\Gamma_1^c)-E(\Gamma_{15}^v)\ \ (\text{polar})\ ,$$

$$\Delta E_c^p=E(\Gamma_{15}^c)-E(\Gamma_1^c)\ \ (\text{polar})\ ,$$

and Δ_0^p (>0) is the energy of the splitoff valence band at Γ in the polar solid.

We now turn our attention to the second method of calculating the momentum matrix elements. Here, we use the empirical tight-binding form of the wave functions,[7] and then use the orbital wave functions of Huang and Ching[16] to calculate the matrix elements. The momentum matrix elements take the form

$$\mathbf{p}_{ij}(\mathbf{k})=N_p\sum_{m,n}\Omega_m^b\Omega_n^a U_{im}^* W_{jn}\sum_{\Delta\mathbf{R}}\langle b^m(0)\mid\mathbf{p}\mid a^n(\Delta\mathbf{R})\rangle e^{i\mathbf{k}\cdot\Delta\mathbf{R}}\ , \tag{17}$$

where $\mid b^m(0)\rangle$ is a bond orbital located at the origin pointing in one of the four bonding directions, $\mid a^m(\Delta\mathbf{R})\rangle$ is an antibonding orbital located at an fcc lattice site $(\Delta\mathbf{R})$ pointing in one of the four bonding directions, U_{im}, W_{jn} are the eigenvectors which diagonalize the 4×4 valence or conduction-band Hamiltonians, respectively, Ω_m^b, Ω_m^a are normalization constants for the bonding and antibonding basis states, and N_p is the atomic density. There is a corresponding equation for the c-c' matrix elements. The bonding and antibonding orbitals can be written in terms of the sp^3 hybrids in the usual way[7] and the hybrids, in turn, are linear com-

binations of the s and p orbitals on a particular atomic site. For the sp orbitals, we use the results obtained by Huang and Ching[16] with their semi-*ab-initio* tight-binding calculation. We use only the valence s and p orbitals, consistent with the minimal sp^3 basis set approach used by the empirical tight-binding method. We feel justified in neglecting the d (or core-state) orbitals in the determination of the momentum matrix elements for two reasons. First, the inclusion of d-type orbitals is not consistent with the dependence of the matrix elements on lattice constant, which is seen in the next section to predict the experimental effective masses fairly well. Second, the d-type orbitals are much more localized than the s or p orbitals,[16] and hence the contribution of the d-type orbitals is expected to be small.

The s,p orbitals are of the form[16]

$$S_{\mathrm{I,II}}(\mathbf{r})=\sum_i \{C^S_{\mathrm{I,II}}\}_i e^{-\alpha_i r^2}, \qquad P^x_{\mathrm{I,II}}(\mathbf{r})=x\sum_i \{C^P_{\mathrm{I,II}}\}_i e^{-\alpha_i r^2}, \tag{18}$$

where I,II refers to the location (i.e., on an anion or cation) of the orbital, the α_i are a set of Gaussian exponents ranging from $\alpha_1=0.15$ to $\alpha_{14}=250\,000$, r is in units of Bohr radii, and there are corresponding equations for $P^y(\mathbf{r})$ and $P^z(\mathbf{r})$. The use of Gaussian orbitals makes the calculation of the various momentum matrix elements between the localized orbitals analytic. In order to evaluate the matrix element in Eq. (17), two additional parameters are required,[7] the polarity α_p and hybrid overlap parameter, S. The overlap parameter is calculated directly from the given orbitals, and the polarity values are taken from our ETB results.[7] The values of various parameters for all materials are shown in Table I. The polarities arrived at in that paper agreed fairly well with values from other sources[16,23] and, in any case, the v-c matrix elements did not vary significantly when the polarity was changed by as much as 30%. The c-c' matrix elements showed a stronger dependence on polarity as expected (since they vanish in the limit of zero polarity); however, as will be seen in the next section, the dependence on polarity is much weaker than what would be required to account for the difference between the calculated and experimental values of the c-c' matrix elements. The sum in Eq. (17) is carried out to convergence, which included up to the seventh nearest-neighbor contributions for all materials. The bands are calculated using the empirical tight-binding method, and so the eigenvectors in Eq. (17) in general are dependent on that model. However, at the Brillouin zone center the eigenvectors are determined by symmetry and are therefore model independent.

The last method for determining the v-c type matrix elements is to evaluate the sum in Eq. (17) only to a particular nearest neighbor, and then adjust the matrix elements at the BZ center so that the calculated value of $\epsilon_1(0)$ agrees with experiment. The matrix elements are evaluated to the D nearest-neighbor bonds as defined in Ref. 7. This is necessary to yield reasonable values for the ratio of the v-c and v-c' matrix elements, since only one adjustment constant was used for all v-c type matrix elements. We now present the results of the calculations.

V. RESULTS

We briefly review the results for the ETB calculation[7] of the linear-optical properties, before presenting the results of this paper. The overall agreement in Ref. 7 between theory and experiment for the dispersion in $\epsilon_2(\omega)$ was found to be fairly good for GaP, GaAs, and GaSb; however, the results for InAs and InSb were not as good. A common discrepancy in the conduction bands was the position of the maximum in the lowest conduction band in the (100) direction. This maximum typically occurred too close to the zone boundary and had the combined effect of decreasing the E_2 peak in $\epsilon_2(\omega)$ and increasing the effective mass (and hence the density of states) at the Γ_2^c point. This last effect produced a rise in $\epsilon_2(\omega)$ at the band edge which was sharper than the observed increase, and was most prominently seen in InAs. We defer further discussion of the bands until the presentation of the results for the dispersion in $\vec{\vec{\chi}}^{(2)}$. We now turn our attention to the values obtained for the momentum matrix elements, and the zero-frequency values for $\vec{\vec{\chi}}^{(2)}$.

A. Momentum matrix elements and $\vec{\vec{\chi}}^{(2)}(0)$

Table II shows the results for the matrix elements obtained by the three methods outlined in Sec. IV, and Table III shows the experimental and calculated conduction-band effective masses. From Table III, it is clear that the empirical method of determining the matrix elements (method 1) succeeds fairly well in predicting the experimental effective masses in the polar materials. Generally, the effective masses are overestimated, indicating that perhaps either the v-c matrix elements

TABLE I. Various parameters for the materials studied. The bond polarity (α_p) is taken from Ref. 7.

	Material parameters				
Element	GaP	GaAs	GaSb	InAs	InSb
$\epsilon_1(0)$ (expt.)	9.1	10.9	14.4	12.3	15.7
Hybrid overlap	0.70	0.65	0.64	0.62	0.60
Bond polarity (α_p)	0.52	0.50	0.44	0.53	0.41
Lattice constants (Å)	5.451	5.658	6.095	6.050	6.470

TABLE II. Momentum matrix elements determined by the three methods outlined in the text.

	Matrix[b] element	Matrix elements[a] Experiment, method 1	Theory, method 2	Theory, method 3
GaP	v_0-c'		0.184	0.388
	v-c	0.629	0.299	0.438
	v-c'	0.525	0.374	0.561
	c-c'	0.294	0.011	
GaAs	v_0-c'		0.249	0.321
	v-c	0.616	0.367	0.422
	v-c'	0.520	0.369	0.435
	c-c'	0.242	0.020	
GaSb	v_0-c'		0.257	0.277
	v-c	0.575	0.371	0.371
	v-c'	0.508	0.359	0.366
	c-c'	0.229	0.031	
InAs	v_0-c'		0.238	0.193
	v-c	0.561	0.368	0.279
	v-c'	0.510	0.353	0.273
	c-c'	0.279	0.088	
InSb	v_0-c'		0.259	0.190
	v-c	0.533	0.388	0.275
	v-c'	0.500	0.339	0.243
	c-c'	0.239	0.050	

[a]Shown here are the magnitude of the matrix elements in units of $(\hbar/a_b)$.
[b]Matrix elements are defined as follows. v_0-$c' \equiv |\langle \Gamma_1^v | \mathbf{p} | \Gamma_{15}^c \rangle|$; v-$c \equiv |\langle \Gamma_{15}^v | \mathbf{p} | \Gamma_1^c \rangle|$; v-$c' \equiv |\langle \Gamma_{15}^v | p | \Gamma_{15}^c \rangle|$; c-$c' \equiv |\langle \Gamma_1^c | \mathbf{p} | \Gamma_{15}^c \rangle|$.

are underestimated, or that the c-c' matrix elements are slightly overestimated, as obtained by method 1. From Table II, it is seen that the values of the v-c matrix elements calculated from the orbitals (method 2) in general agree reasonably well with the values obtained by fitting $\epsilon_1(0)$ (method 3), and these values are in turn consistently ~ 20–30% lower than the experimental values. In the case of InAs and InSb, the matrix elements obtained by fitting $\epsilon_1(0)$ are reduced relative to the calculated matrix elements. The dispersion in $\epsilon_2(\omega)$ for InAs and InSb is not reproduced as well by the empirical band structure, and so for these elements, $\epsilon_1(0)$ is overestimated and the matrix elements determined by fitting $\epsilon_1(0)$ are consequently underestimated. Other calculations,[24,25] which give good agreement between theory and experiment for $\epsilon_1(0)$, do not explicitly state the calculated values for the momentum matrix elements. In our case, if the calculated values of the matrix elements are used, fairly good agreement between theory and experiment would result for $\epsilon_1(0)$, except for InAs and InSb.

The values obtained for the c-c' matrix elements, on the other hand, are consistently smaller than the experimentally determined values by, in some cases, over an order of magnitude. The exact reason for this discrepancy is not clear, except that in general tight-binding methods produce better results for valence bands than for conduction bands.

We turn now to the zero-frequency limit of $\vec{\vec{\chi}}^{(2)}$. Table IV shows our results for the theoretical calculation, along with the results from other calculations and the experimental values. Our values for $\vec{\vec{\chi}}^{(2)}$ were obtained by using the v-c matrix elements determined by

TABLE III. Effective masses at the Γ_1^c point. The calculated values were obtained using Aspnes' (Ref. 13) interpolation formulas for P, Q, and $E(\Gamma_{15'}^c)$ (for homopolar materials), together with band energies from Ref. 24.

	Effective masses at Γ_1^c					
Compound	GaP	GaAs	GaSb	InP	InAs	InSb
m^*/m (Expt.)[a]	0.13[b]	0.070	0.047	0.073	0.026	0.015
m^*/m (Calc.)	0.12	0.078	0.070	0.089	0.026	0.022

[a]From Ref. 15.
[b]This is the calculated value from Ref. 15, there being no experimental data for this element.

TABLE IV. Theoretical and experimental results for $\vec{\chi}^{(2)}(0)$.

	Results for $\vec{\chi}^{(2)}(0)$[a]				
Element	GaP	GaAs	GaSb	InAs	InSb
Our theory	38	96	230	450	920
Fong and Shen		4.0		12.5	3.0
Aspnes	24	38	70	64	110
Expt.[b]	52	90	300	200	330[c]
Expt.[d]	20	43			
Expt.[e]	20	34	115	76	230

[a] $\vec{\chi}^{(2)}(0)$ is expressed in units of 1×10^{-8} esu.
[b] From Ref. 26.
[c] From Ref. 3. Note that this value was measured at $\lambda=1.06$ μm.
[d] From Ref. 27.
[e] Obtained by using Levine and Betheas' (Ref. 27) revised estimate of $\chi^{(2)}_{123}(0)$ for GaP, together with the relative measurements of Ref. 26. The data for InSb were obtained by using the revised value of $\chi^{(2)}_{36}(0)$ for KDP from Ref. 27 together with the data from Ref. 3.

method 3 and the c-c matrix elements determined by method 1. The results of $\vec{\chi}^{(2)}(0)$ for GaP, GaAs, and GaSb agree quite well with the data from Ref. 26, while the value for InAs is overestimated by a factor of ~2. The value of $\vec{\chi}^{(2)}(0)$ for InSb is not known, since the experimental value[3] was measured at $\lambda=1.06$ μm. In this range, the theory agrees in overall magnitude with experiment; presumably, however, the overestimate of $\vec{\chi}^{(2)}(0)$, as seen for InAs, occurs for InSb as well. This overestimate of $\vec{\chi}^{(2)}(0)$ for InAs and InSb arises from the same features in the band structure which cause $\epsilon_1(0)$ to be overestimated—namely that the contribution of the E_0 optical peaks is too large, owing to the conduction bands being too flat at the Γ point. Even though this is partially compensated for in the v-c matrix elements by fitting $\epsilon_1(0)$, $\vec{\chi}^{(2)}$ is much more sensitive to deficiencies in the band structure. From Table IV it is evident that our values for $\vec{\chi}^{(2)}(0)$ overestimate the experimental results of Ref. 27 for GaP and GaAs, which are claimed to be more accurate than previous results. In addition, if the revised absolute value of $\vec{\chi}^{(2)}(0)$ for GaP is used to rescale the relative measurements of Ref. 26, the values of $\vec{\chi}^{(2)}(0)$ for the other elements are decreased by roughly a factor of 2.5. If the lower values for $\vec{\chi}^{(2)}(0)$ were correct, it would imply that either the contribution from the $E_0(\Gamma)$ optical peak for GaP, GaAs, and GaSb is overestimated (although not to the extent that it is for InAs and InSb), or that the experimental values of the c-c matrix elements are too large. Probably both factors are responsible since, as we will see in the next section, even for GaAs the contribution of the E_0 optical peak is somewhat larger in our theory than in FS's; in addition, an overestimate of the experimental c-c' matrix elements seems possible, since the experimental v-c matrix elements were also larger than the matrix elements determined by fitting $\epsilon_1(0)$. The results of Aspnes[13] were obtained by replacing the band energy denominator in Eq. (7) with an average value equal to the E_1 optical peak energy, and agree quite well with the lower experimental values in Table IV. If these lower values for $\vec{\chi}^{(2)}(0)$ were correct, it would imply that the major contribution to $\vec{\chi}^{(2)}(0)$ does indeed come from the E_1 optical peak.

In any case, all of the calculated values for $\vec{\chi}^{(2)}(0)$ are comparable to, or larger than, all of the experimental values. This is in contrast to the results of FS which, for GaAs, InAs, and InSb, were all at least an order of magnitude too small. They attributed this to the neglect of local-field corrections; however, as seen from Table II, if the calculated values for the c-c' matrix elements are used, we would obtain values for $\vec{\chi}^{(2)}(0)$ which would be comparable to FS's results. Since FS do not state their values for the momentum matrix elements, we must consider this a possible explanation for their discrepancy, rather than the supposed local-field corrections. One further point we wish to make is that local-field effect calculations in silicon[14] show that the value of $\epsilon_1(0)$ is actually *decreased* by 10–15%, not increased as the simplistic use of local-field correction factors for insulating solids would predict.[28]

Finally, we mention that $\vec{\chi}^{(2)}(0)$ was calculated both by using the LATM to evaluate $\vec{\chi}^{(2)''}$ and then using the Kramers-Kronig relations to obtain $\vec{\chi}^{(2)'}(\omega)$, and also by evaluating $\vec{\chi}^{(2)'}(0)$ directly from Eq. (7) (taking the bands to be constant over a particular tetrahedron). For all elements the second result was found to agree with the first, to within 5% for GaP, GaAs, GaSb, $\sim15\%$ for InAs, and by $\sim20\%$ for InSb. The increase of this difference for InAs and InSb reflects the fact that the bands vary more rapidly (the effective mass at Γ is smaller) for these elements than the other elements. In addition, $\vec{\chi}^{(2)}(0)$ was calculated both by assuming that the matrix elements were constant (taken to be their values at the Γ point), and also by allowing the matrix elements to vary over the Brillouin zone. For all elements, the difference in $\vec{\chi}^{(2)}(0)$ for these two methods was on the order of 5%.

B. Dispersion in $\vec{\chi}^{(2)}(\omega)$

We now turn our attention to the calculations of the dispersion in $\vec{\chi}^{(2)}$. We discuss results for GaAs, GaSb, InAs, and InSb and simply present results for GaP, for which no dispersion measurements exist.

Figure 2(a) shows the results for $|\vec{\vec{\chi}}^{(2)}(\omega)|$ for GaAs, as well as experimental data from various sources. In general, the agreement between theory and experiment for GaAs is quite good (in view of the variation of the experimental data), particularly the prediction of the large dip near 2.2 eV and even the shoulder at ~2.5 eV. [The scale for the theoretical curve in Fig. 2(a) has been adjusted slightly to match the peaks of $|\vec{\vec{\chi}}^{(2)}(\omega)|$, but still yields a value for $\vec{\vec{\chi}}^{(2)}(0)$ which is within the experimental limits.] One significant difference between FS's results and ours is that in our case the first peak at ~0.75 eV, due to the 2ω resonance with the direct band gap at Γ (E_0 peak in the linear-optical spectrum), is much more pronounced. This is due to the fact that the density of states at Γ_1^c is higher than it should be. The peak at ~1.5 eV is also larger in our case, being comparable to the two large peaks at ~2.2 and ~2.8 eV. To understand this feature, we show the real and imaginary parts of $\vec{\vec{\chi}}^{(2)}(\omega)$ in Fig. 2(b). Also, the contributions of the 2ω [$\sim\delta(E_{ji}-2\hbar\omega)$] and ω [$\sim\delta(E_{ji}-\hbar\omega)$] terms to $\vec{\vec{\chi}}^{(2)\prime\prime}$ for the band numbers $i=3,4$, $j=5$, $l=6$ (where i refers to the valence bands and j,l refer to the conduction bands, and the bands are numbered in increasing order of energy) are shown in Fig. 2(c), as well as the contribution of the 2ω term to $\vec{\vec{\chi}}^{(2)\prime\prime}$ for $i=3,4$, $j=6$, and $l=5$. We call these three terms, terms 1, 2, and 3, respectively. The fact that the contribution from term 1 is always positive, whereas term 2 has oscillations, can be

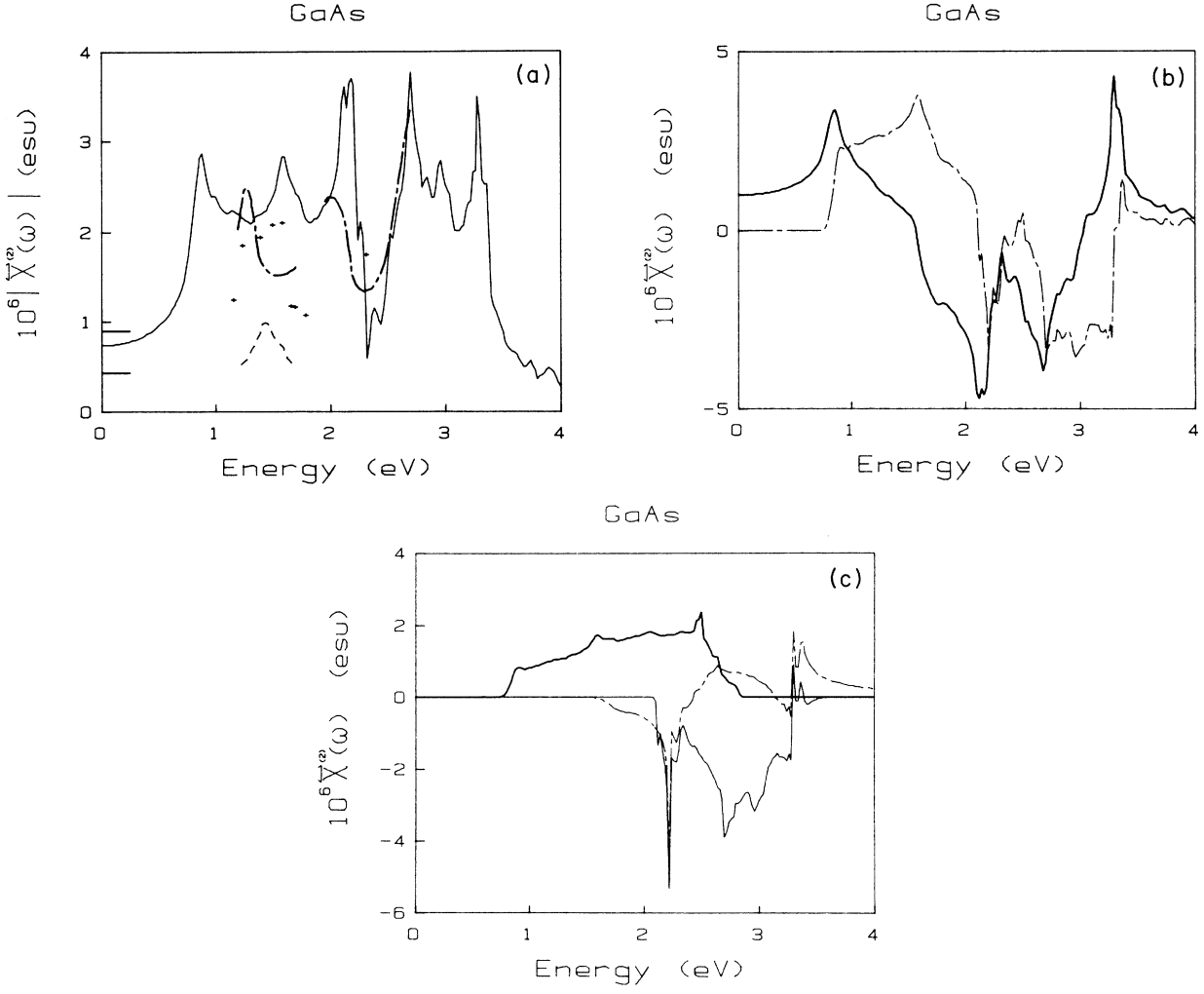

FIG. 2. Results of $\vec{\vec{\chi}}^{(2)}$ calculations for GaAs. (a) Theoretical and experimental results for $|\vec{\vec{\chi}}^{(2)}(\omega)|$. The experimental results from 1.95–2.7 eV are from Ref. 6, the results from 1.1–1.7 eV (dashed-dotted line) are from Ref. 4, the results from 1.2–1.8 eV (dashed line) are from Ref. 5, and the data points denoted by + are from Ref. 3. The data from Ref. 5 are in arbitrary units. The bars near zero frequency indicate the two experimental results listed in Table IV. The relative data in Refs. 3, 4, and 6 were converted to absolute units with the revised values of $\vec{\vec{\chi}}^{(2)}(0)$ for potassium dihydrogen phosphate (KDP), ammonia dihydrogen phosphate (ADP), and quartz, from Ref. 27. For all figures, the element of $\vec{\vec{\chi}}^{(2)}(\omega)$ shown is $\chi^{(2)}_{123}$, the only independent element for cubic materials. (b) Real (solid line) and imaginary (dashed line) parts of $\vec{\vec{\chi}}^{(2)}(\omega)$. (c) Contributions from various terms to $\vec{\vec{\chi}}^{(2)\prime\prime}$. The thick solid line is the 2ω contribution for bands $i=3,4$, $j=5$, $l=6$, and the dashed line is the ω contribution for the same bands. The solid line is the 2ω contribution for bands $i=3,4$, $j=6$, $l=5$.

easily understood from Eq. (5b). The contribution from the 2ω term is positive because there are (by definition) no bands between the lowest conduction band and the upper valence band, and so the denominator is positive. For the ω term, on the other hand, the denominator will change sign whenever the second conduction band crosses the 2ω point, which most noticeably happens along the (100) direction before the peak in the lowest conduction band. This feature was discussed in Sec. II, where it was pointed out that this is distinct from a double resonance (as defined in that section).

For GaAs, from Fig. 2(c), we see that the peak at 1.5 eV in $\vec{\chi}^{(2)}$ is in fact predominantly due to the 2ω resonance with the E_1 optical peak (from the critical point along the Λ direction) and not from the ω resonance with the E_0 optical peak (at the Γ point) in agreement with FS's conclusion. The peak at 2 eV is shifted down relative to FS's results, and in fact is in closer agreement with experiment. FS attribute this peak to the 2ω contribution of the E_2 optical peak, along (100) [or simply $\Delta^{(2\omega)}(4-5)$, where 4 and 5 are the band indices in order of increasing energy]. Figure 2(c) shows that the contribution of term 1 does show a peak at ~ 2.3 eV, but in our case this peak is actually responsible for the dip in $|\vec{\chi}^{(2)}|$, as it interferes destructively with the $\Delta^{(\omega)}(4-5)$ contribution and the $\Lambda^{(2\omega)}(4-6)$ contribution. The large peak at ~ 2.7 eV in Fig. 2(a) arises mainly from the $\Delta^{(2\omega)}(4-6)$ contribution, and much less from the $\Lambda^{(\omega)}(4-5)$ contribution, in partial agreement with FS's results. Note that the contribution of $\Delta^{(2\omega)}(4-6)$ (term 3) in Fig. 2(c) is predominantly negative because the matrix element product is negative, since $j=6$, $l=5$.

We now turn to the theoretical results for InAs and InSb, shown in Fig. 3. The most striking feature in $|\vec{\chi}^{(2)}(\omega)|$ is the presence of the large peak around ~ 0.25 eV and ~ 0.15 eV for InAs and InSb, respectively. This peak is due to the contribution of the 2ω and ω terms at Γ (E_0 optical peak) from the lowest conduction band. Its large magnitude is due to the lower effective

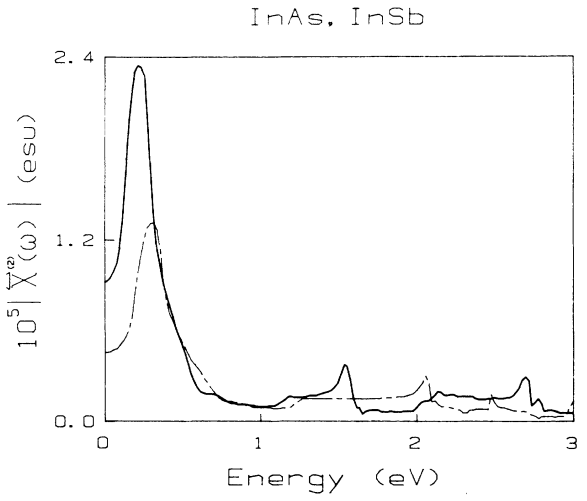

FIG. 3. Theoretical results for $|\vec{\chi}^{(2)}(\omega)|$ for InAs (dashed line) and InSb (solid line).

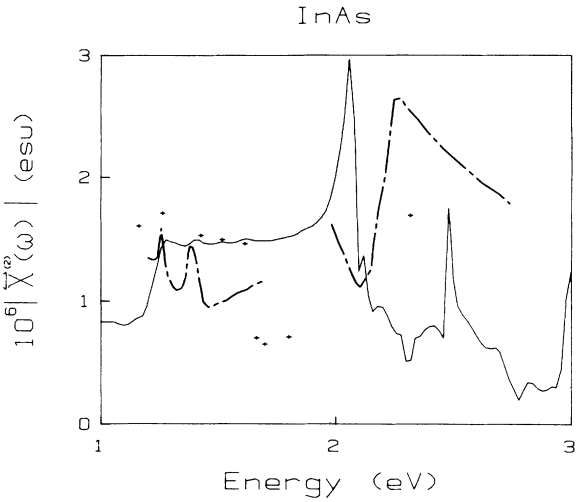

FIG. 4. Theoretical and experimental results of $|\vec{\chi}^{(2)}(\omega)|$ for InAs. The experimental results from 1.1–1.7 eV are from Ref. 4, the results from 1.95–2.7 eV are from Ref. 6, and the data denoted by + are from Ref. 3.

mass (and consequently, higher density of states) at the Γ point than what is obtained from more accurate band structures, combined with the $1/E^5$ dependence of the response function. This is also responsible for $\vec{\chi}^{(2)}(0)$ being significantly larger than the experimental result for InAs (and presumably for InSb as well). Because the band gap is smaller for InSb than InAs, the effect is even larger for InSb and hence the value for $\vec{\chi}^{(2)}(0)$ is further enhanced. How large the peaks actually are, however, is not known since the experimental data [Fig. 5(b)] do not cover this range. At frequencies where the effect of this large peak is absent, the theory in fact agrees quite well with experiment, in terms of the overall magnitude of $\vec{\chi}^{(2)}(0)$ (cf. Figs. 4 and 5). The theoretical curve for $|\vec{\chi}^{(2)}(\omega)|$, along with the experimental data, is shown in Fig. 4 for InAs. The shoulder near 1.2 eV arises from the 2ω contribution of the E_1 optical peak, as FS found. The fact that our results do not show two peaks reflects the fact that we have ignored spin orbit coupling in this calculation. The peak at ~ 2.0 eV arises from the ω contribution of the E_1 optical peak, as well as the 2ω contribution from the E_2 optical peak (along Δ). This last contribution extends out to ~ 2.8 eV.

The theoretical and experimental results for InSb are shown in Fig. 5. While our results seem to agree with the peak near 1.5 eV as observed in Ref. 3, the data from Ref. 4 disagree sharply with this. In any event, we direct our attention to the band-structure origins of the structure in $\vec{\chi}^{(2)}(\omega)$. The shoulder at ~ 1.2 eV is due to the 2ω resonance with the E_1 optical peak, as FS found. The large peak in Fig. 5(a) at ~ 1.5 eV arises from two sources, as seen from Fig. 5(c). There is a contribution from the ω term at the E_1 optical peak (Λ) shifted down from ~ 1.9 eV where it appears in other band structures,[24] and a contribution from the 2ω resonance with the E_2 optical peak which is shifted down from ~ 2.2 eV where it appears in FS's results. The contribution from

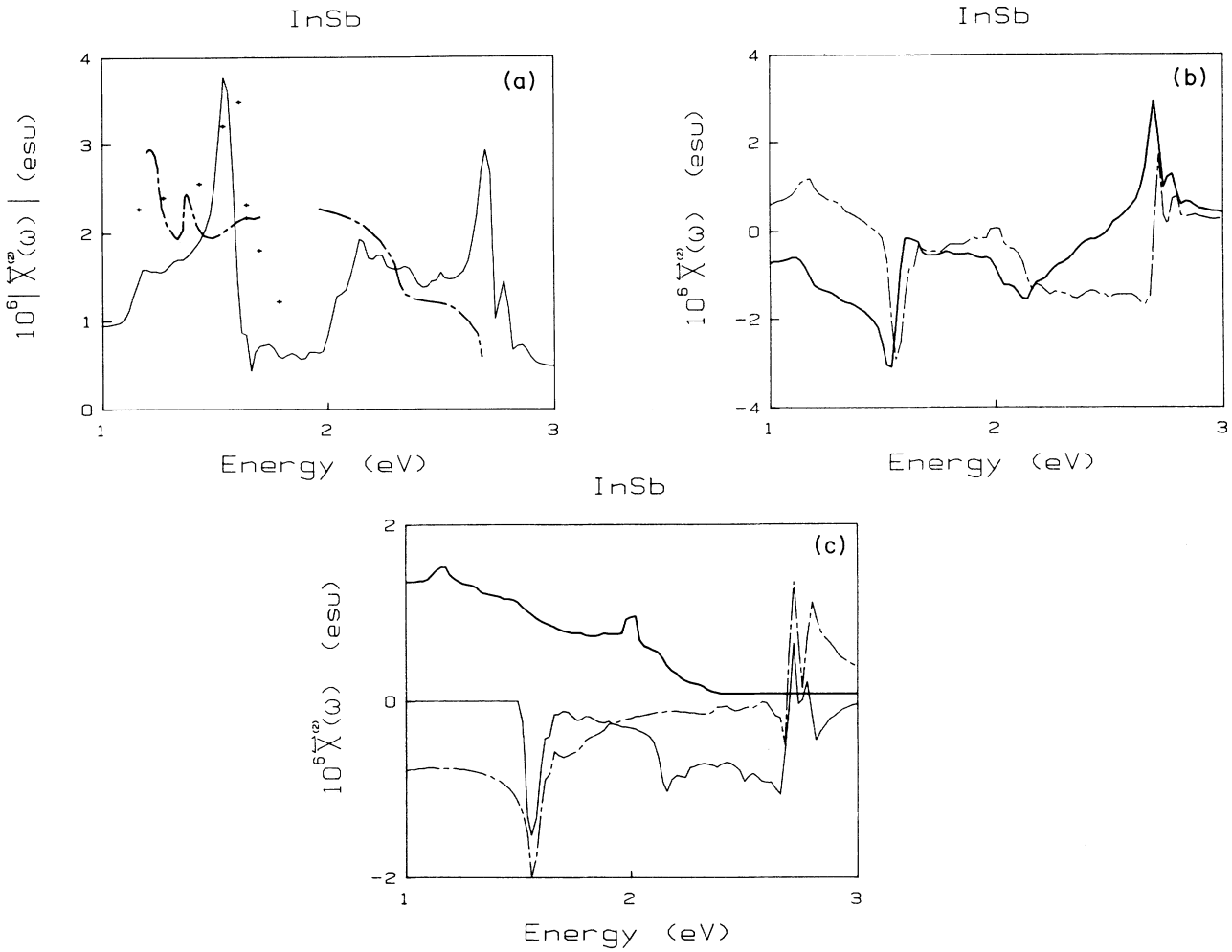

FIG. 5. Results of $|\vec{\chi}^{(2)}(\omega)|$ for InSb. (a) Theoretical and experimental results for $|\vec{\chi}^{(2)}(\omega)|$. The experimental results are from the same sources as in Fig. 4. (b) Real (solid line) and imaginary (dashed line) parts of $\vec{\chi}^{(2)}(\omega)$. (c) Contributions of various terms to $\vec{\chi}^{(2)''}$. The thick solid and dashed lines are the 2ω and ω terms, respectively, contribution for bands $i=3,4$, $j=5$, $l=6$. The solid line is the contribution of the 2ω term for bands $i=3,4$, $j=6$, $l=5$.

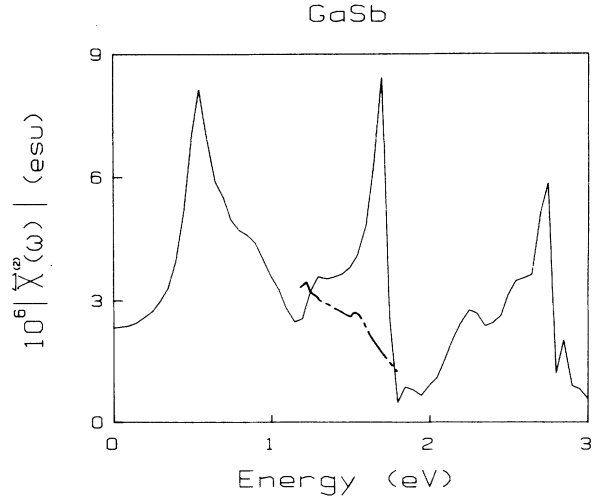

FIG. 6. Theoretical and experimental results of $|\vec{\chi}^{(2)}(\omega)|$ for GaSb. The experimental results (dashed-dotted line) are from Ref. 5 and are in arbitrary units.

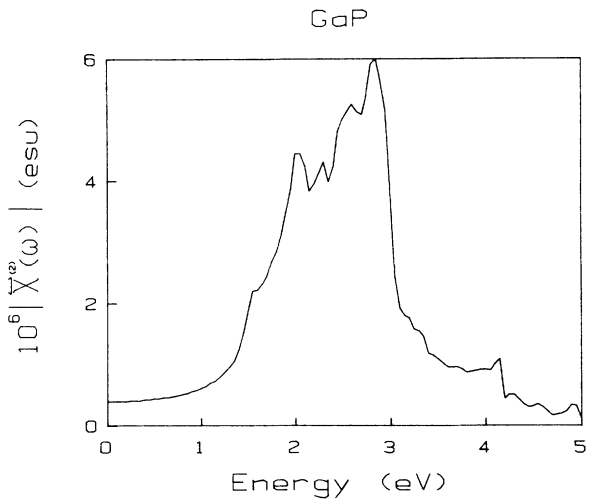

FIG. 7. Theoretical results of $|\vec{\chi}^{(2)}(\omega)|$ for GaP.

the second piece is shifted because the second conduction band is lower than that of the pseudopotential bands in the (100) direction. The large size of the peak at 1.5 eV in Fig. 5(a) could be due to a double resonance enhancement, as FS claim, except shifted down slightly in our case. The broad peak at 2.0–2.7 eV is primarily due to the 2ω resonance with the E_2 optical peak from the second conduction band.

Figure 6 shows the results for GaSb, for which only one set of experimental results exists.[5] The data in that paper are in arbitrary units, and so comparison of the absolute magnitude of $\vec{\chi}^{(2)}$ is not possible. The experimental data do not show the large peak at ~ 1.5 eV as seen in the theory; however, the actual second-harmonic signal in Ref. 5 does show a substantial peak, which presumably is canceled out by variations in the linear dielectric properties. Any error in the values for the linear dielectric properties would result in substantial changes in the structure of $\vec{\chi}^{(2)}(\omega)$, as pointed out by the authors.[5] For completeness, we also present the results for $|\vec{\chi}^{(2)}(\omega)|$ for GaP (Fig. 7) even though experimental data only exist, to our knowledge, near zero frequency.

We see therefore that for GaAs, where the linear-optical properties were reproduced well by the band structure, good agreement is also found between theory and experiment for $\vec{\chi}^{(2)}$. For InAs and InSb, where the linear-optical spectrum was not reproduced as well, the discrepancies in the spectrum of $\vec{\chi}^{(2)}$ are further enhanced. This demonstrates that the spectrum of $\vec{\chi}^{(2)}(\omega)$ is much more sensitive to fine details in the band structure than are the linear-optical properties.

VI. CONCLUSIONS

We have used an empirical tight-binding band-structure technique to calculate both the dispersion and zero-frequency limit of $\vec{\chi}^{(2)}(\omega)$ for zinc-blende crystals. This was accomplished by first evaluating the imaginary part of $\vec{\chi}^{(2)}(\omega)$ using an extension of the linearized analytic tetrahedra method, and then using the Kramers-Kronig relations to obtain the real part of $\vec{\chi}^{(2)}(\omega)$.

The results for $\vec{\chi}^{(2)}(\omega)$ show that when the v-c momentum matrix elements obtained by fitting $\epsilon_1(0)$ to experiment are used with the experimental c-c' momentum matrix elements, good agreement is found with experiment for most materials. Both InAs and InSb yielded results for $\vec{\chi}^{(2)}(0)$ which were larger than experiment, and this was attributed to the inability of the tight-binding model to adequately reproduce the correct band structure. In all cases, values obtained for $\vec{\chi}^{(2)}(0)$ were comparable to, or larger than, the experimental values, contrary to FS's results. We feel that their results could be due to calculated values for the momentum matrix elements—in particular the c-c' matrix elements—which are too small. Indeed, FS point out that the calculated linear reflectivity for InSb was $\sim 20\%$ too low. In any case, it is evident that local-field corrections, at least in the form appropriate for insulators, do not play a significant role in determining the magnitude of $\vec{\chi}^{(2)}(0)$ for these materials.

In addition, it was found that the values for the valence-band–conduction band momentum matrix elements obtained by fitting $\epsilon_1(0)$ agreed fairly well with the calculated matrix elements. Both of these values were found to be consistently 20–30 % lower than the experimental values, obtained by using the experimental effective masses in conjunction with $\mathbf{k}\cdot\mathbf{p}$ perturbation theory and Cardona's empirical antisymmetric perturbation model. This discrepancy is too large to be accounted for by inaccuracies in the band structure, since the linear-optical absorption spectrum is reproduced fairly well for most materials. At the present time, we cannot suggest the reason for this difference.

Experimental data in the literature for the dispersion in $\vec{\chi}^{(2)}(\omega)$ vary substantially, and so comparison between theory and experiment is somewhat difficult. Notwithstanding this, our theoretical results agree reasonably well with experiment over the ranges where experimental data exist. This demonstrates that a simple tight-binding band-structure approach towards covalent solids can indeed be used to calculate dispersion in nonlinear-optical properties and conversely, that with the improvement of experimental data, the nonlinear-optical spectrum can be used as a more sensitive test of band-structure theories than $\epsilon_2(\omega)$.

ACKNOWLEDGMENTS

We wish to thank Professor W. Y. Ching for providing us with his data for the tight-binding orbitals. We also acknowledge financial support of this work from the Natural Sciences and Engineering Research Council of Canada, including additional financial support for D.J.M. One of us (H.M.vD.) gratefully acknowledges financial support from the John Guggenheim Foundation.

[1]M. I. Bell, in *Electronic Density of States,* Natl. Bur. Stand. (U.S.) Spec. Publ. No. 323, edited by L. H. Bennet (U.S. GPO, Washington, D.C., 1971), p. 757.

[2]C. Y. Fong and Y. R. Shen, Phys. Rev. B **12**, 2325 (1975).

[3]R. K. Chang, J. Ducuing, and N. Bloembergen, Phys. Rev. Lett. **15**, 415 (1965).

[4]F. G. Parsons and R. K. Chang, Opt. Commun. **3**, 173 (1971).

[5]H. Lotem, G. Koren, and Y. Yacoby, Phys. Rev. B **9**, 3532 (1974).

[6]D. Bethune, A. J. Schmidt, and Y. R. Shen, Phys. Rev. B **11**, 3867 (1975).

[7]D. J. Moss, E. Ghahramani, J. E. Sipe, and H. M. van Driel, Phys. Rev. B **34**, 8758 (1986).

[8]G. Lehmann and M. Taut, Phys. Status Solidi B **54**, 469 (1972).

[9]D. J. Moss, J. E. Sipe, and H. M. van Driel, Phys. Rev. B **36**, 1153 (1987).

[10]C. Flytzanis and J. Ducuing, Phys. Rev. **178**, 1218 (1969).

[11]J. C. Phillips and J. A. Van Vechten, Phys. Rev. **183**, 709 (1969).
[12]B. F. Levine, Phys. Rev. B **7**, 2600 (1973).
[13]D. E. Aspnes, Phys. Rev. B **6**, 4648 (1972).
[14]S. G. Louie, J. R. Chelikowsky, and M. L. Cohen, Phys. Rev. Lett. **34**, 155 (1975); W. R. Hanke and L. J. Sham, *ibid.* **33**, 582 (1974).
[15]M. Cardona, J. Phys. Chem. Solids **24**, 1543 (1963).
[16]M. Z. Huang and W. Y. Ching, J. Phys. Chem. Solids **46**, 977 (1985).
[17]P. N. Butcher and T. P. McLean, Proc. Phys. Soc. London **81**, 219 (1963); **83**, 579 (1964).
[18]D. J. Moss, J. E. Sipe, and H. M. van Driel, J. Opt. Soc. Am. B **3**, 94 (1986).
[19]C. Flytzanis, *Quantum Electronics,* edited by H. Rabin and C. L. Tang (Academic, New York, 1975), Vol. IA, p. 9.
[20]W. J. Caspers, Phys. Rev. **133**, A1249 (1964); P. J. Price, *ibid.* **130**, 1792 (1963).
[21]D. E. Aspnes, Bull. Am. Phys. Soc. **16**, 46 (1971).
[22]E. O. Kane, J. Phys. Chem. Solids **8**, 38 (1959).
[23]W. A. Harrison and S. Ciraci, Phys. Rev. B **10**, 1516 (1974).
[24]J. R. Chelikowsky and M. L. Cohen, Phys. Rev. B **14**, 556 (1976).
[25]C. S. Wang and B. M. Klein, Phys. Rev. B **24**, 3393 (1981); *ibid.* **24**, 3417 (1981).
[26]J. J. Wynne and N. Bloembergen, Phys. Rev. **188**, 1211 (1969).
[27]B. F. Levine and C. G. Bethea, Appl. Phys. Lett. **20**, 272 (1972).
[28]N. Bloembergen, *Nonlinear Optics* (Benjamin, Reading, Mass., 1965), p. 68.